

## **Clothe CsPbI<sub>3</sub> perovskite in robust phase-pure armor to boost the thermal stability**

Xue Tan<sup>a</sup>, Shubin Wang<sup>a\*</sup>, Qixian Zhang<sup>a</sup>, Hailiang Wang<sup>a</sup>, Huicong Liu<sup>a</sup>, Weiping Li<sup>a</sup>, Liqun Zhu<sup>a</sup>, Tinglu Song<sup>b</sup>,  
Zhenhua Cui<sup>c</sup>, Yang Bai<sup>c</sup>, Haining Chen<sup>a\*</sup>

a. School of Materials Science and Engineering, Beihang University, No. 37 Xueyuan Road, Haidian District, Beijing 100083, People's Republic of China.

b. Experimental Center of Advanced Materials, School of Materials Science & Engineering, Beijing Institute of Technology, Beijing 100081, People's Republic of China.

c. Beijing Key Laboratory of Construction Tailorable Advanced Functional Materials and Green Applications, MIIT Key Laboratory for Low-dimensional Quantum Structure and Devices, Experimental Center of Advanced Materials, School of Materials Science & Engineering, Beijing Institute of Technology, Beijing 100081, People's Republic of China.  
\*E-mail: shubinwang@buaa.edu.cn; chenhaining@buaa.edu.cn

## Supporting information

**Materials:**

CsI (99.9%), PbI<sub>2</sub> (99.99%) and DMAI (99.5%) was purchased from Xi'an Polymer Light Technology Corp. DMF (99.8%, extra dry) was purchased from Acros Organics. Titanium diisopropoxide bis(acetylacetonate) (75 wt. % in isopropanol) were purchased from TCI (Shanghai) Development Co., Ltd. Commercial TiO<sub>2</sub> paste (30 NR-D) was purchased from Dyesol company. 1-Butanol (99%) and ethanol (99.5%) were purchased from Shanghai Aladdin Biochemical Technology Co. Ltd. The carbon paste (DD-20) was purchased from Guangzhou Seaside Technology Co. ltd. All chemicals were used as-received without further purification.

**Deposition of TiO<sub>2</sub> films:**

FTO glass was cleaned with successive sonication in deionized water, ethanol and isopropanol. TiO<sub>2</sub> blocking layer was then spin coated onto FTO glass at 2000 rpm for 20 s, using a titanium diisopropoxide bis(acetylacetonate) solution in 1-butanol (0.15 M), and then heated at 120 °C for 5 min. TiO<sub>2</sub> mesoporous scaffolds were deposited by spin coating at 5000 rpm for 30 s using a commercial TiO<sub>2</sub> paste dispersed in ethanol, followed by sintering at 100 °C for 5 min and then at 550 °C for 30 min.

**Deposition of perovskite films:**

Precursor solutions were prepared by mixing DMAI, PbI<sub>2</sub> and CsI in DMF. The molar ratio of DMAI: PbI<sub>2</sub>: CsI was 1.5:1.5:1 and the concentration of CsI in the solution was set at 1 M. The intermediate films were deposited by spin coating the precursor solution on substrate at 2000 rpm for 20 s, followed by heating at 100 °C for 30s. For the CsPbI<sub>3</sub> film, the intermediate film was directly annealed at 220 °C for 5 min without other treatments. For the IT CsPbI<sub>3</sub> film, the intermediate film was treated with the isopropanol solution of QCDI and then annealed at 220 °C for 5 min. The PT CsPbI<sub>3</sub> film was obtained by treating the surface of the final CsPbI<sub>3</sub> film with the QCDI solution and then annealed at 100 °C for 5 min. For the QCdPbI<sub>3</sub> film, the solution of QCDI and PbI<sub>2</sub> with equal moles dissolved in DMF/DMSO (1:1) was spin-coated on FTO substrate and then annealed at 150 °C for 5 min. For the DMAPbI<sub>3</sub> film, the solution of DMAI and PbI<sub>2</sub> with equal moles dissolved in DMF was spin-coated on FTO substrate and then annealed at 150 °C for 5 min. For the Cs<sub>4</sub>PbI<sub>6</sub> film, the solution of CsI and PbI<sub>2</sub> with molar ratio of 4:1 dissolved in DMF was spin-coated on FTO substrate and then annealed at 150 °C for 5 min.

**Deposition of carbon electrodes:**

For fabricating C-PSCs, carbon electrode was directly painted on the perovskite films at room temperature, followed by annealing at 100 °C for 20 min. The whole procedure was conducted in dry air atmosphere.

**Characterizations:**

X-ray diffraction (XRD) patterns were obtained by a Rigaku D/MAX-2500 X-ray diffractometer with an X-ray tube Cu K<sub>α</sub> radiation. ( $\lambda = 1.5406 \text{ \AA}$ ). Chemical states of film surface were evaluated by an X-ray photoemission spectroscopy (XPS, ESCALab250Xi). Ultraviolet-visible-infrared spectrophotometer (UV-vis) absorption spectra were recorded on a Shimadzu UV-3600 ultraviolet-visible spectrometer. Scanning electron microscopy (SEM) images and EDS were obtained on a SUPRA55 SEM at an accelerating voltage of 5 kV. Surface roughness of these films were characterized by a Bruker Dimension ICON atomic force microscopy (AFM). TOF-SIMS measurement was performed using a PHI NanoTOF II instrument (ULVAC-PHI, Inc.), where an Argon gas beam was used for erosion and a 30 keV Bi<sup>+</sup> pulsed primary ion beam was used for the analysis.

Steady-state photoluminescence (PL) spectra were recorded on a Nanolog FL3-2iHR (Horiba Jobin Yvon Ltd) with an excitation wavelength of 340 nm. Time-resolved PL (TRPL) spectra taken on an ultrafast lifetime Spectrofluorometer (Delta flex) and a 475 nm ultrafast laser was used as the excitation light source. Confocal photoluminescence (PL) maps were recorded on a laser scanning confocal microscope (A1R-si).

The photovoltaic performance was tested under a solar light simulator (Newport Oriel Sol 3A, model number 94063A, AM 1.5 global filter) in ambient air. The light intensity was calibrated to 1 Sun (100 mW/cm<sup>2</sup>) using an Oriel reference solar cell (monocrystalline silicon) and meter. The active area of cells was masked at around 6.25 mm<sup>2</sup>. Current density-voltage (*J-V*) curves, dependence of *J<sub>sc</sub>* and *V<sub>oc</sub>* on light intensity, Dark *J-V* measurement of the electron-only device and Mott-Schottky curves were measured on ZENNIUM pro electrochemical workstation (ZAHNER-Elektrik GmbH & Co., KG, Germany). The film stability tests were performed in air atmosphere (RH 10~20 %) at room temperature (~25 °C), in humid air (RH 80~90 %) at room temperature (~25 °C), and in N<sub>2</sub> (RH < 10%) at 85 °C. The device stability tests were performed by storing non-encapsulated devices in air atmosphere (RH 10~20 %) at room temperature (~25 °C) and in N<sub>2</sub> (RH < 10%) at 85 °C. *J-V* curves were measured periodically in ambient air atmosphere (RH 30~80 %) to track the device performance.

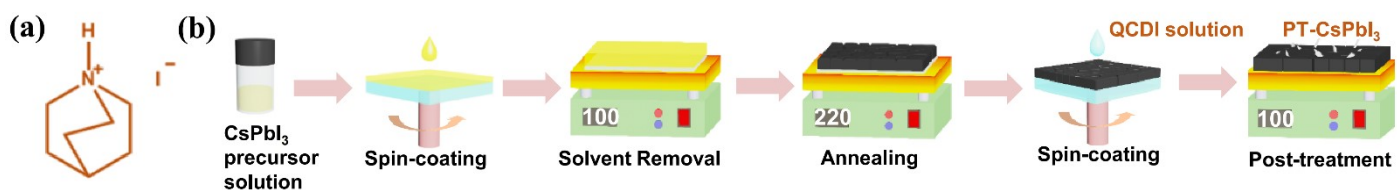


**Figure S1.** (a) Molecular structure of QCDI; (b) Schematic diagram of the fabrication procedure for the PT-CsPbI<sub>3</sub> film.

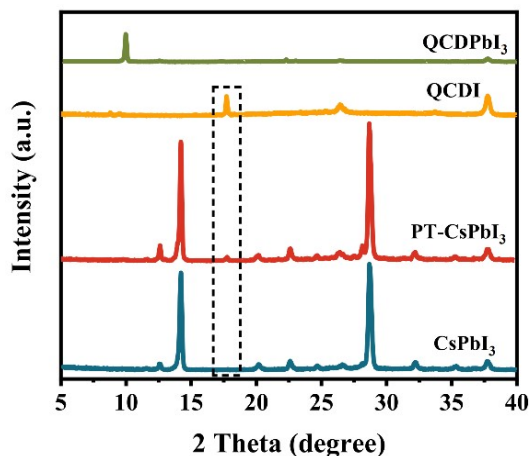


**Figure S2.** XRD patterns of the QCDPbI<sub>3</sub>, QCDI, CsPbI<sub>3</sub> and PT-CsPbI<sub>3</sub> films.

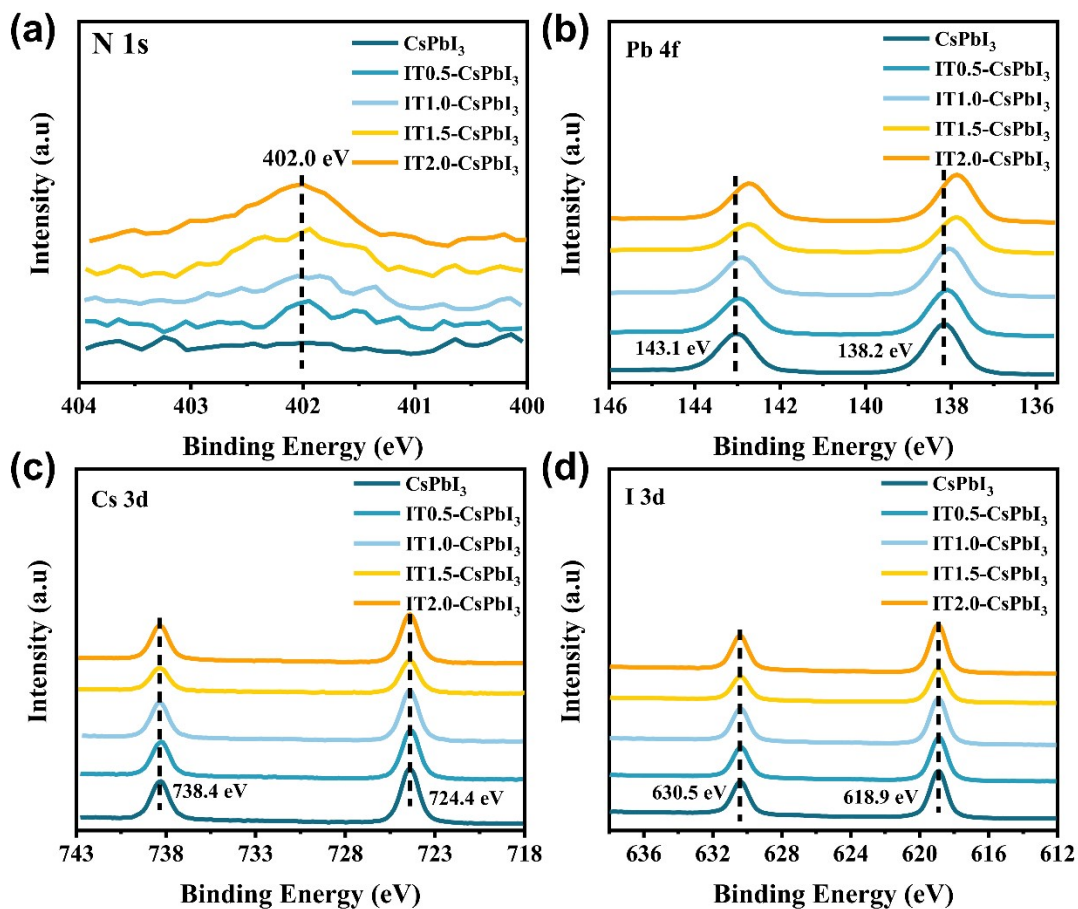


**Figure S3.** XPS spectra of (a) N 1s, (b) Pb 4f and (c) Cs 3d, and (d) I 3d of the IT-CsPbI<sub>3</sub> films with increasing amount of QCDI.

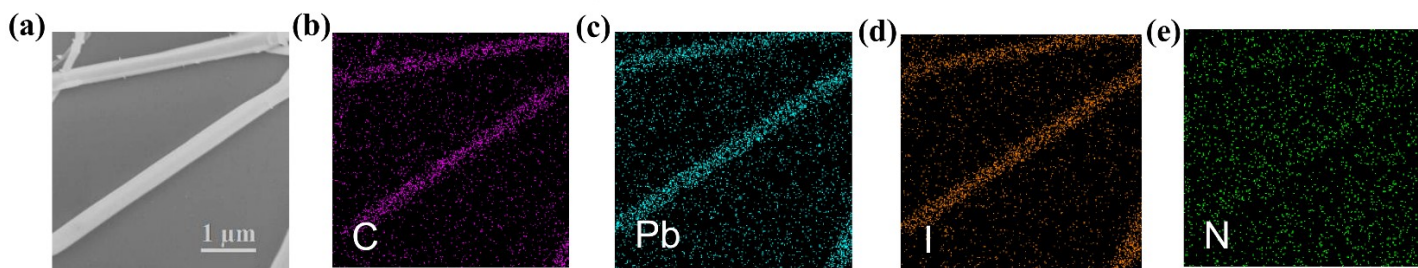


**Figure S4.** (a) Top-view SEM image and EDS mapping of (b) C element, (c) Pb element, (d) I element, and (e) N element distribution of the QCDPbI<sub>3</sub> film.

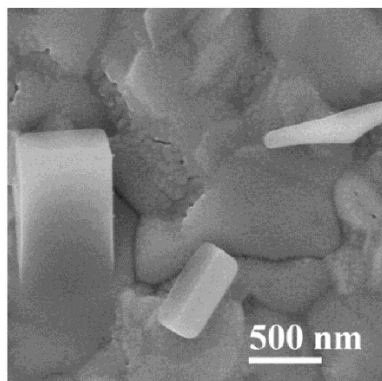


**Figure S5.** Top-view SEM image of the PT-CsPbI<sub>3</sub> film.

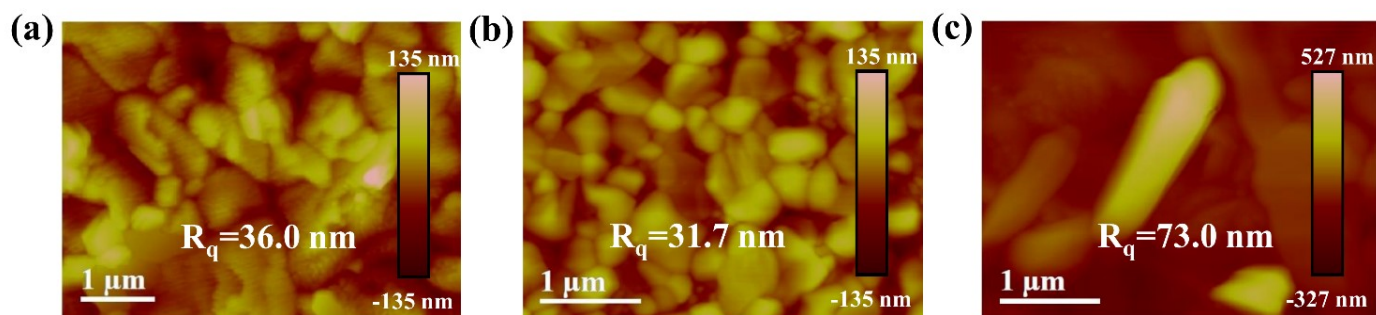


**Figure S6.** AFM images of (a) CsPbI<sub>3</sub>, (b) IT-CsPbI<sub>3</sub> and (c) PT-CsPbI<sub>3</sub> films.

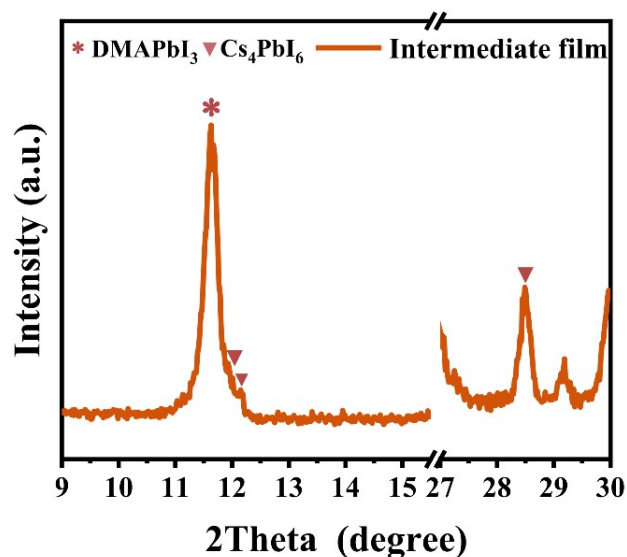


Figure S7. XRD patterns of the intermediate film.

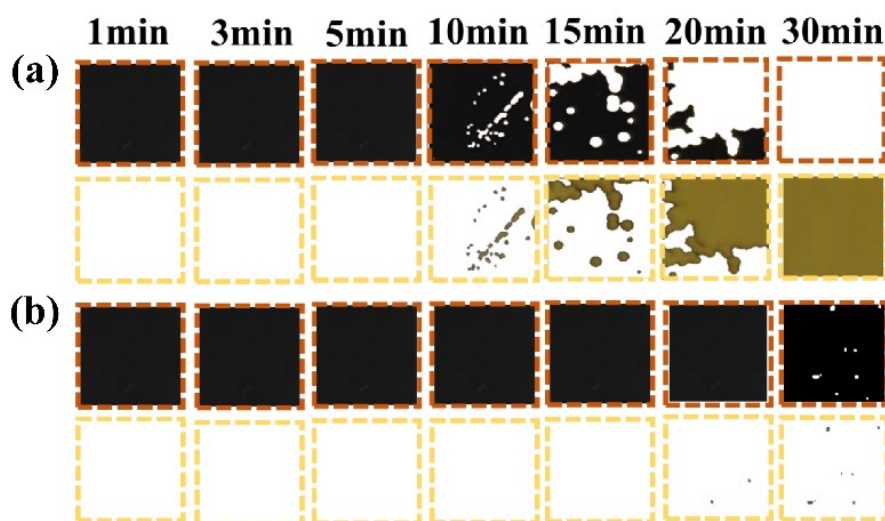


Figure S8. The separated black and yellow regions of photographs in Figure 3(a).

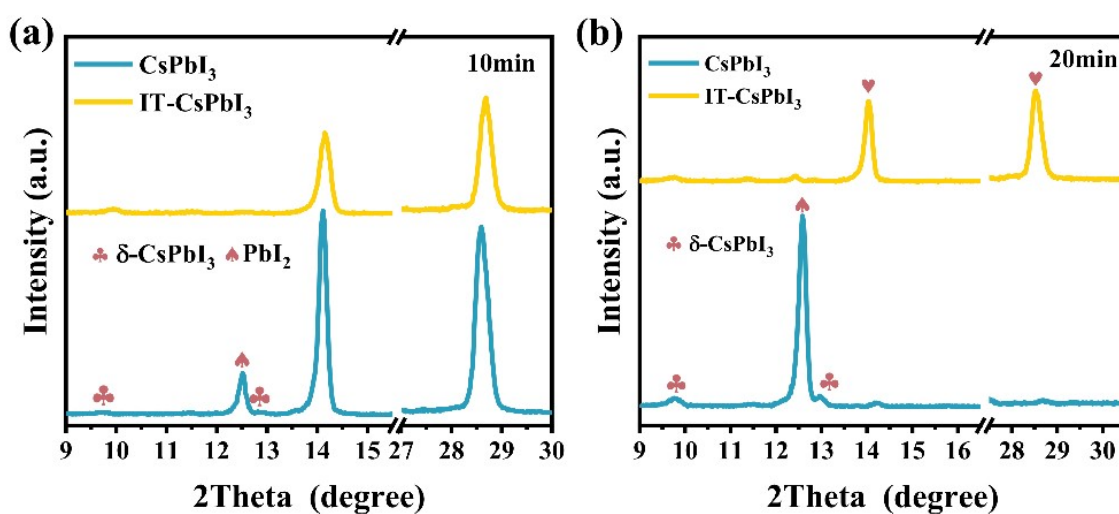
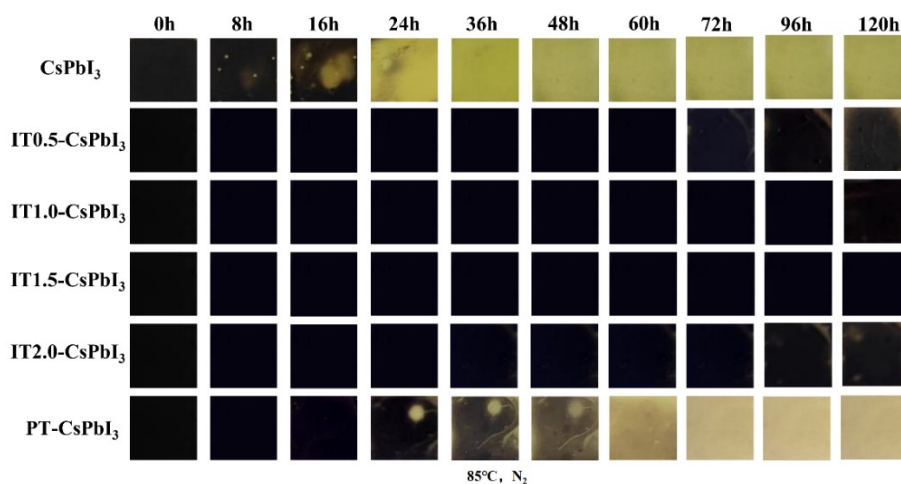
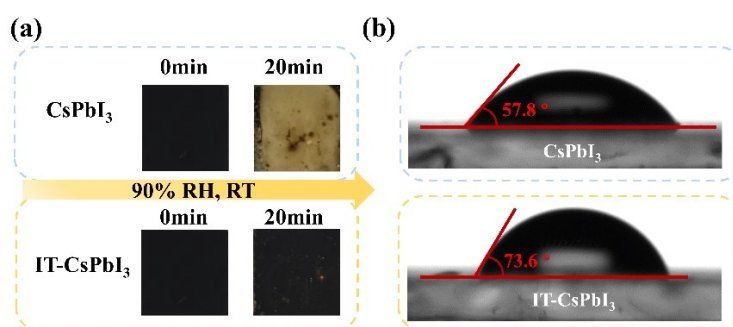


Figure S9. XRD patterns of the pristine CsPbI<sub>3</sub> and IT-CsPbI<sub>3</sub> film when annealing for (a) 10 min and (b) 20min.



**Figure S10.** Photographs the CsPbI<sub>3</sub>, IT-CsPbI<sub>3</sub> and PT-CsPbI<sub>3</sub> films heated at 85°C in N<sub>2</sub> glovebox with increasing time.



**Figure S11.** (a) Photographs of the CsPbI<sub>3</sub> and IT-CsPbI<sub>3</sub> films before and after exposed to 90% RH at RT for 20 min; (b) Contact angles of the CsPbI<sub>3</sub> and IT-CsPbI<sub>3</sub> films.

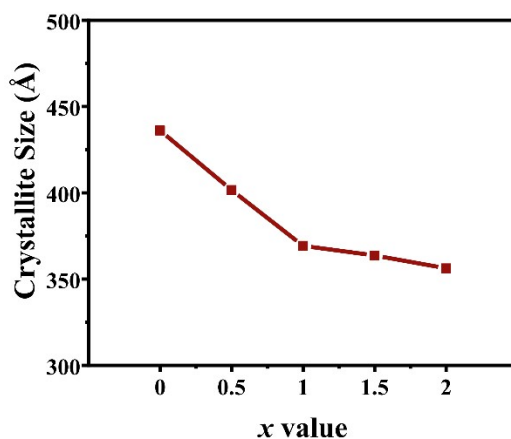


**Figure S12.** Crystallite sizes of *p*-CsPbI<sub>3</sub> with increasing *x* value in the IT*x*-CsPbI<sub>3</sub> films.

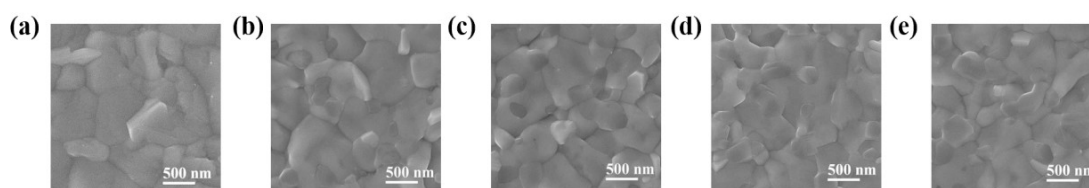


**Figure S13.** Top-view SEM images of the (a) CsPbI<sub>3</sub>, (b) IT0.5-CsPbI<sub>3</sub>, (c) IT1.0-CsPbI<sub>3</sub>, (d) IT1.5-CsPbI<sub>3</sub>, and (e) IT2.0-CsPbI<sub>3</sub> films.

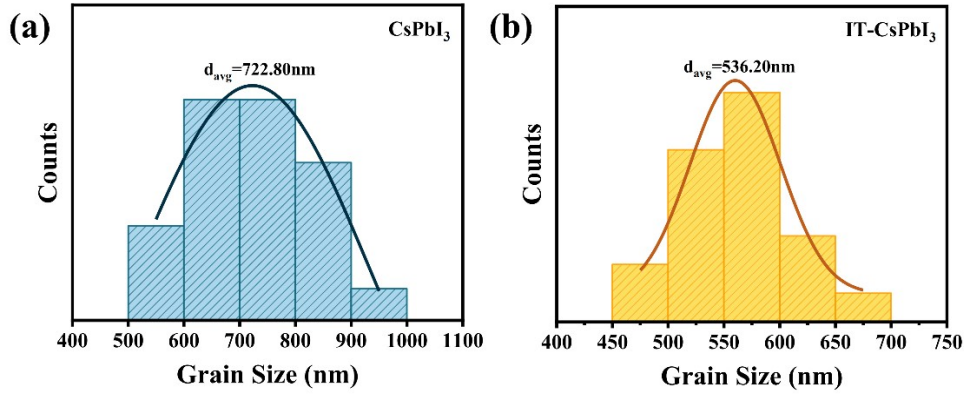


Figure S14. Counted grain sizes of the (a) CsPbI<sub>3</sub> and (b) IT1.5-CsPbI<sub>3</sub> films from corresponding SEM images.

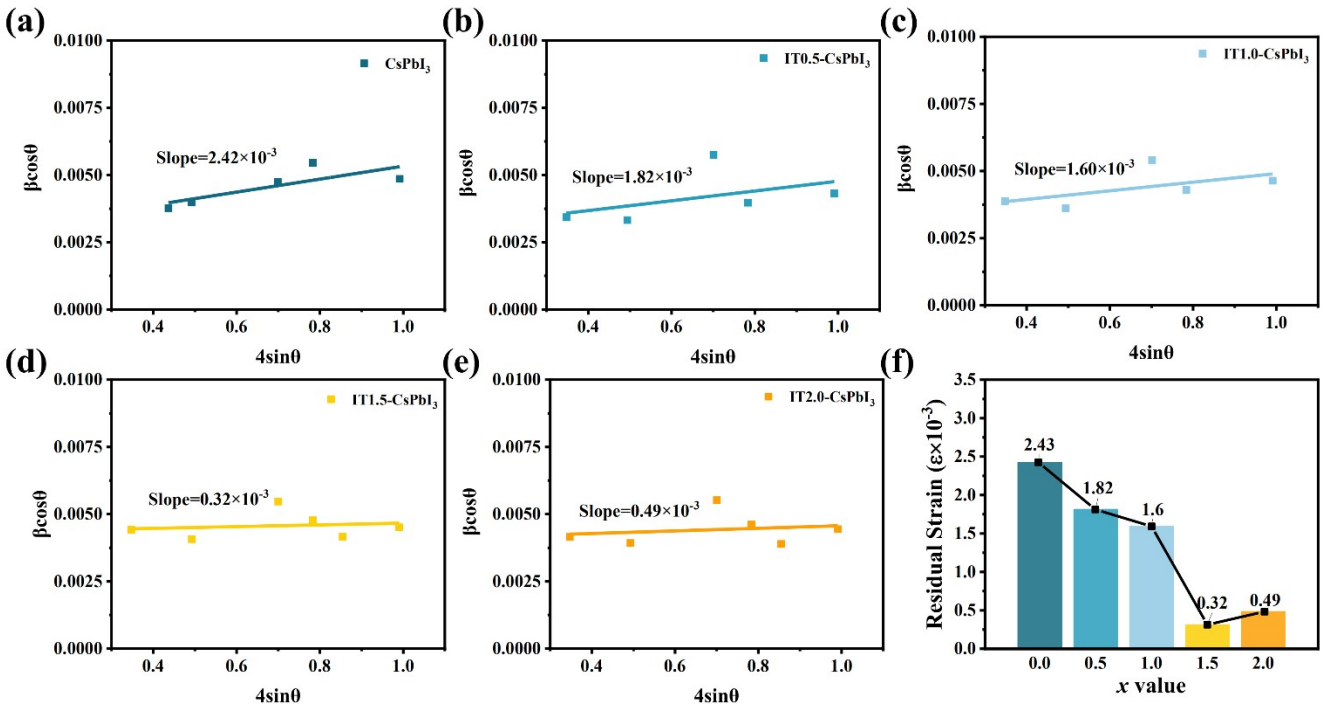


Figure S15. (a)-(e) Williamson-Hall plots and (f) the residual strain of the CsPbI<sub>3</sub> and IT<sub>x</sub>-CsPbI<sub>3</sub> films.

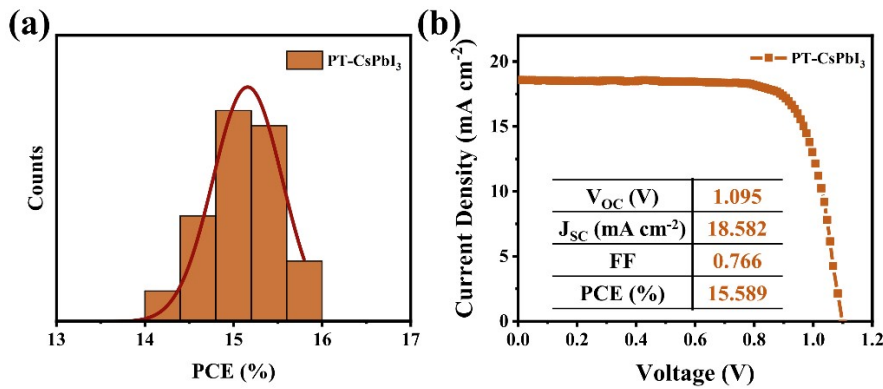
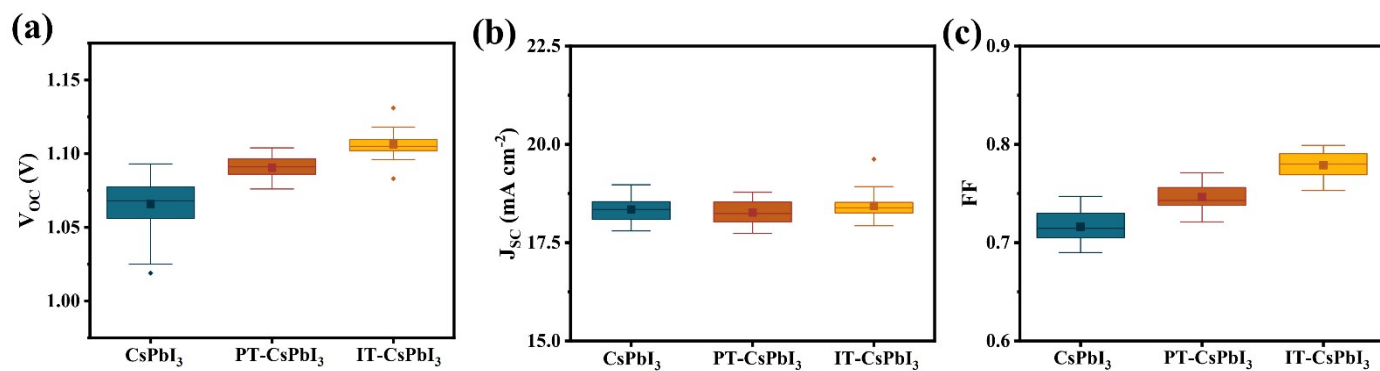
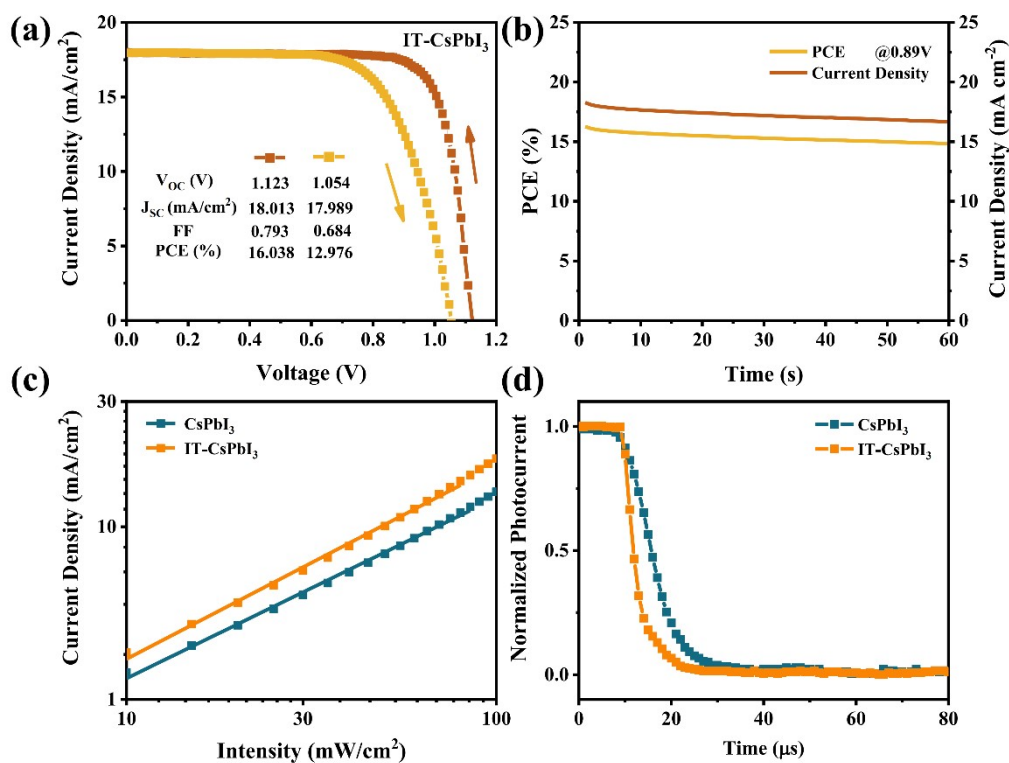


Figure S16. (a) Statistical data of PCEs and (b)  $J-V$  curves of the PT-CsPbI<sub>3</sub> devices.



**Figure S17.** Statistical data obtained from CsPbI<sub>3</sub>, PT-CsPbI<sub>3</sub> and IT-CsPbI<sub>3</sub> C-PSCs: (a)  $V_{OC}$ , (b)  $J_{SC}$ , (c) FF.



**Figure S18.** Other photovoltaic performance of C-PSCs. (a)  $J$ - $V$  curves under forward and reverse scans, (b) steady-state power output, and (c) TPC curves.

**Table S1.** The peak position of the characteristic peaks of *p*-CsPbI<sub>3</sub>.

Sample	CsPbI <sub>3</sub>	IT0.5-CsPbI <sub>3</sub>	IT1.0-CsPbI <sub>3</sub>	IT1.5-CsPbI <sub>3</sub>	IT2.0-CsPbI <sub>3</sub>
(110) plane	14.196°	14.252°	14.263°	14.255°	14.256°
(220) plane	28.756°	28.766°	28.763°	28.775°	28.775°

**Table S2.** The d-spacings (Å) of perovskite phase of the pristine CsPbI<sub>3</sub> and IT-CsPbI<sub>3</sub> films.

Sample	CsPbI <sub>3</sub>	IT0.5-CsPbI <sub>3</sub>	IT1.0-CsPbI <sub>3</sub>	IT1.5-CsPbI <sub>3</sub>	IT2.0-CsPbI <sub>3</sub>
(110) plane	3.141	3.129	3.127	3.128	3.128
(220) plane	1.601	1.601	1.601	1.600	1.600

**Table S3.** The grain sizes (nm) of the pristine CsPbI<sub>3</sub> and IT-CsPbI<sub>3</sub> films.

Sample	CsPbI <sub>3</sub>	IT0.5-CsPbI <sub>3</sub>	IT1.0-CsPbI <sub>3</sub>	IT1.5-CsPbI <sub>3</sub>	IT2.0-CsPbI <sub>3</sub>
Grain Size	722.80±57.63	614.85±37.55	560.74±51.88	536.20±34.07	572.62±41.27

**Table S4.** The fitting results of carrier lifetimes  $\tau$  (ns) for the pristine CsPbI<sub>3</sub> and IT-CsPbI<sub>3</sub> films.

	A <sub>1</sub>	$\tau_1$	A <sub>2</sub>	$\tau_2$	$\tau$
CsPbI <sub>3</sub>	0.668	5.513	0.429	5.514	5.513
IT-CsPbI <sub>3</sub>	1.662	4.061	0.117	63.127	34.972

**Table S5.** Performance comparison of existing C-PSCs based on CsPbX<sub>3</sub> inorganic perovskites.

Perovskite layer	Device structure	$V_{OC}$ (V)	$J_{SC}$ (mA/cm <sup>2</sup> )	FF	PCE (%)	Ref
CsPbI <sub>3</sub>	FTO/c-TiO <sub>2</sub> /m-TiO <sub>2</sub> / CsPbI <sub>3</sub> : Br /carbon	1.03	12.46	0.56	7.22	[1]
	FTO/c-TiO <sub>2</sub> /m-TiO <sub>2</sub> /CsPbI <sub>3</sub> /carbon	0.67	14.31	1.48	4.65	[2]
	FTO/c-TiO <sub>2</sub> /m-TiO <sub>2</sub> /CsPbI <sub>3</sub> /carbon	0.73	14.65	0.5	5.31	[3]
	FTO/c-TiO <sub>2</sub> /m-TiO <sub>2</sub> /CsPbI <sub>3</sub> /CuSCN/carbon	0.94	13.8	0.52	6.9	[4]
	FTO/c-TiO <sub>2</sub> /m-TiO <sub>2</sub> /CsPbI <sub>3</sub> /carbon	0.91	15.76	0.66	9.39	[5]
	FTO/c-TiO <sub>2</sub> /m-TiO <sub>2</sub> /CsPbI <sub>3</sub> /carbon	0.79	18.5	0.65	9.5	[6]
	FTO/c-TiO <sub>2</sub> /m-TiO <sub>2</sub> / Cs <sub>0.95</sub> Na <sub>0.05</sub> PbI <sub>3</sub> /carbon	0.92	16.5	0.703	10.7	[7]
	FTO/c-TiO <sub>2</sub> /m-TiO <sub>2</sub> /CsPbI <sub>3</sub> /PEI-CNT/carbon	0.80	18.58	0.71	10.55	[8]
	FTO/c-TiO <sub>2</sub> /m-TiO <sub>2</sub> /CsPbBr <sub>3</sub> / CsPbI <sub>3</sub> NCs/carbon	1.490	8.66	0.732	9.45	[9]
	FTO/c-TiO <sub>2</sub> /m-TiO <sub>2</sub> /CsPbI <sub>3</sub> : Br: InI <sub>3</sub> /carbon	1.20	15.68	0.64	12.04	[1]
CsPbI <sub>2</sub> Br	FTO/c-TiO <sub>2</sub> /m-TiO <sub>2</sub> /CsPbI <sub>3</sub> /carbon	1.056	17.47	0.79	14.60	[10]
	FTO/c-TiO <sub>2</sub> /CsPbI <sub>2</sub> Br/carbon	1.15	13.54	0.642	10	[11]
	FTO/TiO <sub>2</sub> /CsPbI <sub>2</sub> Br/P3HT-MWCNT/carbon	1.21	13.35	0.62	10.01	[12]
	ITO/SnO <sub>2</sub> /KOH/CsPbI <sub>2</sub> Br/carbon	14.24	1.20	0.687	11.78	[13]
	FTO/Ni <sub>2</sub> O <sub>5</sub> /Cs <sub>0.99</sub> Rb <sub>0.01</sub> PbI <sub>2</sub> Br/carbon	1.24	14.02	0.69	12.00	[14]
	FTO/c-TiO <sub>2</sub> /m-TiO <sub>2</sub> /CsPbI <sub>2</sub> Br/carbon	1.210	14.94	0.73	13.13	[15]
	FTO/Ni <sub>2</sub> O <sub>5</sub> /CsPbI <sub>2</sub> Br/carbon	1.20	13.96	0.66	11.02	[14]
	ITO/SnO <sub>2</sub> /Nb-CsPbI <sub>2</sub> Br/carbon	1.20	12.06	0.72	10.42	[16]
	FTO/SnO <sub>2</sub> /CsPbI <sub>2</sub> Br/carbon	1.23	15.46	0.64	12.19	[17]
	ITO/SnO <sub>2</sub> /CsPbI <sub>2</sub> Br/carbon	1.187	12.91	0.661	10.13	[18]
	ITO/SnO <sub>2</sub> /CsPbI <sub>2</sub> Br/carbon	1.14	14.25	0.641	10.44	[19]
ITO/SnO <sub>2</sub> /CsPbI <sub>2</sub> Br/PMMA/carbon	1.20	12.64	0.71	10.95	[20]	
ITO/SnO <sub>2</sub> /CsPbI <sub>2</sub> Br/Co <sub>3</sub> O <sub>4</sub> /carbon	1.19	13.09	0.82	11.21	[21]	

	FTO/c-TiO <sub>2</sub> /CsPbI <sub>2</sub> Br/carbon	1.207	16.62	0.74	14.84	[22]
	FTO/c-TiO <sub>2</sub> /CsPbI <sub>2</sub> Br/Carbon	1.15	13.87	0.64	10.21	[23]
CsPbIBr <sub>2</sub>	ITO/SnO <sub>2</sub> /CsPbIBr <sub>2</sub> /carbon	1.23	8.50	0.67	7.00	[24]
	FTO/ c-TiO <sub>2</sub> /m-TiO <sub>2</sub> /CsPbIBr <sub>2</sub> /carbon	0.99	13.15	0.57	7.36	[25]
	FTO/ c-TiO <sub>2</sub> /m-TiO <sub>2</sub> /CsPb <sub>0.9</sub> Sn <sub>0.1</sub> IBr <sub>2</sub> /carbon	1.26	14.30	0.63	11.33	[26]
	FTO/ c-TiO <sub>2</sub> /Li-CsPbIBr <sub>2</sub> /CuPc/carbon	1.22	10.27	0.74	9.25	[27]
	FTO/ ZnO <sub>2</sub> /CsPbIBr <sub>2</sub> /carbon	1.03	11.60	0.63	7.60	[28]
	FTO/ c-TiO <sub>2</sub> /CsPbIBr <sub>2</sub> /carbon	1.245	10.66	0.69	9.16	[29]
	FTO/ c-TiO <sub>2</sub> /CsPbIBr <sub>2</sub> /carbon	1.142	9.11	0.63	6.55	[30]
	FTO/ TiO <sub>2</sub> /CsBr/CsPbIBr <sub>2</sub> /carbon	1.284	10.31	0.52	6.88	[31]
	FTO/ TiO <sub>2</sub> /CsBr/CsPbIBr <sub>2</sub> /carbon	1.261	11.80	0.72	10.71	[20]
	CsPbBr <sub>3</sub>	FTO/c-TiO <sub>2</sub> /m-TiO <sub>2</sub> /CsPbBr <sub>3</sub> /carbon	1.29	5.7	0.68	5.00
FTO/c-TiO <sub>2</sub> /CsPbBr <sub>3</sub> /carbon		1.34	6.46	0.68	5.86	[33]
FTO/c-TiO <sub>2</sub> /m-TiO <sub>2</sub> /CsPbBr <sub>3</sub> /carbon		1.38	7.13	0.62	6.10	[34]
FTO/c-TiO <sub>2</sub> /CsPbIBr <sub>2</sub> /carbon		1.29	12.03	0.70	10.95	[35]
FTO/c-TiO <sub>2</sub> /m-TiO <sub>2</sub> /CsPbBr <sub>3</sub> /carbon		1.24	7.4	0.73	6.7	[36]
FTO/TiO <sub>2</sub> /CsPbBr <sub>3</sub> /carbon		1.19	7.48	0.688	6.12	[37]
FTO/c-TiO <sub>2</sub> /m-TiO <sub>2</sub> /CsPbBr <sub>3</sub> /P3HT/carbon		1.36	7.02	0.68	6.49	[38]
FTO/Ni-TiO <sub>2</sub> /CsPbBr <sub>3</sub> /CuPc/carbon		1.362	7.92	0.793	8.55	[39]
FTO/TiO <sub>2</sub> /SnO <sub>2</sub> /CsPbBr <sub>3</sub> /CuPc/carbon		1.310	8.24	0.814	8.79	[40]
FTO/c-TiO <sub>2</sub> /m-TiO <sub>2</sub> /CsPb <sub>0.995</sub> Zn <sub>0.005</sub> Br <sub>3</sub> /carbon		1.56	7.30	0.806	9.18	[41]
FTO/c-TiO <sub>2</sub> /m-TiO <sub>2</sub> /CsPbBr <sub>3</sub> /CsPbBr <sub>3</sub> NCs/carbon		1.348	7.85	0.744	7.87	[9]
FTO/c-TiO <sub>2</sub> /m-TiO <sub>2</sub> /CsPbBr <sub>3</sub> /P1Z1/carbon		1.578	7.652	0.830	10.03	[42]
FTO/TiO <sub>2</sub> /SnO <sub>2</sub> /CsPbBr <sub>3</sub> /carbon		1.610	7.80	0.844	10.60	[43]
FTO/c-TiO <sub>2</sub> /m-TiO <sub>2</sub> /CsPbBr <sub>3</sub> /carbon		1.594	7.48	0.851	10.14	[44]
FTO/c-TiO <sub>2</sub> /m-TiO <sub>2</sub> /CsPbBr <sub>3</sub> /MnS/carbon		1.52	8.28	0.83	10.45	[1]
FTO/SnO <sub>2</sub> /CsPbBr <sub>3</sub> /carbon		1.622	7.87	0.801	10.71	[45]
FTO/c-TiO <sub>2</sub> /m-TiO <sub>2</sub> /Cu(Cr,Ba)O <sub>2</sub> /CsPbBr <sub>3</sub> /carbon		1.615	7.81	0.855	10.79	[46]
FTO/c-TiO <sub>2</sub> /m-TiO <sub>2</sub> /CsPbBr <sub>3</sub> /QDs/carbon		1.626	7.73	0.863	10.85	[47]
FTO/c-TiO <sub>2</sub> /m-TiO <sub>2</sub> /CsPbBr <sub>3</sub> /carbon		1.431	6.84	0.78	7.62	[48]
FTO/c-TiO <sub>2</sub> /m-TiO <sub>2</sub> /CsPbBr <sub>3</sub> /carbon		1.52	7.56	0.827	9.53	[49]
FTO/c-TiO <sub>2</sub> /m-TiO <sub>2</sub> /CsPbBr <sub>3</sub> /carbon		1.50	7.56	0.830	10.03	[50]
FTO/c-TiO <sub>2</sub> /m-TiO <sub>2</sub> /CsPbBr <sub>3</sub> /carbon		1.458	8.12	0.821	9.72	[51]
FTO/c-TiO <sub>2</sub> /m-TiO <sub>2</sub> /CsPb <sub>0.97</sub> Tb <sub>0.03</sub> Br <sub>3</sub> /SnS:ZnS/NiO <sub>x</sub> /carbon	1.57	8.21	0.796	10.26	[52]	

## References:

- [1] Liang J, Han X, Yang J H, et al. Defect-Engineering-Enabled High-Efficiency All-Inorganic Perovskite Solar Cells [J]. *Advanced materials*, 2019, 31(51): e1903448.
- [2] Liang J, Wang C, Zhao P, et al. Solution synthesis and phase control of inorganic perovskites for high-performance optoelectronic devices [J]. *Nanoscale*, 2017, 9(33): 11841-5.
- [3] Xiang S, Li W, Wei Y, et al. The synergistic effect of non-stoichiometry and Sb-doping on air-stable  $\alpha$ -CsPbI<sub>3</sub> for efficient carbon-based perovskite solar cells [J]. *Nanoscale*, 2018, 10(21): 9996-10004.
- [4] Murugadoss G, Thangamuthu R, Senthil Kumar S M, et al. Synthesis of ligand-free, large scale with high quality all-inorganic CsPbI<sub>3</sub> and CsPb<sub>2</sub>Br<sub>5</sub> nanocrystals and fabrication of all-inorganic perovskite solar cells [J]. *Journal of Alloys and Compounds*, 2019, 787: 17-26.
- [5] Wang H, Xiang S, Li W, et al. Skillfully deflecting the question: a small amount of piperazine-1,4-dium iodide radically enhances the thermal stability of CsPbI<sub>3</sub> perovskite [J]. *Journal of Materials Chemistry C*, 2019, 7(38): 11757-63.
- [6] Xiang S, Fu Z, Li W, et al. Highly Air-Stable Carbon-Based  $\alpha$ -CsPbI<sub>3</sub> Perovskite Solar Cells with a Broadened Optical Spectrum [J]. *ACS Energy Letters*, 2018, 3(8): 1824-31.
- [7] Xiang S, Li W, Wei Y, et al. Sodium Doping Pushes the Efficiency of Carbon-Based CsPbI<sub>3</sub> Perovskite Solar Cells to 10.7 [J]. *iScience*, 2019, 15: 156-64.
- [8] Yang Y, Chen H, Hu C, et al. Polyethyleneimine-functionalized carbon nanotubes as an interlayer to bridge perovskite/carbon for all inorganic carbon-based perovskite solar cells [J]. *Journal of Materials Chemistry A*, 2019, 7(38): 22005-11.
- [9] Su G, He B, Gong Z, et al. Enhanced charge extraction in carbon-based all-inorganic CsPbBr<sub>3</sub> perovskite solar cells by dual-function interface engineering [J]. *Electrochimica Acta*, 2019, 328: 135102.
- [10] Wang H, Liu H, Dong Z, et al. Composition manipulation boosts the efficiency of carbon-based CsPbI<sub>3</sub> perovskite solar cells to beyond 14% [J]. *Nano Energy*, 2021, 84: 105881.
- [11] Dong C, Han X, Zhao Y, et al. A Green Anti-Solvent Process for High Performance Carbon-Based CsPbI<sub>2</sub>Br All-Inorganic Perovskite Solar Cell [J]. *Solar RRL*, 2018, 2(9): 1800139.
- [12] Wang G, Liu J, Chen K, et al. High-performance carbon electrode-based CsPbI<sub>2</sub>Br inorganic perovskite solar cell based on poly (3-hexylthiophene)-carbon nanotubes composite hole-transporting layer [J]. *Journal of colloid and interface science*, 2019, 555: 180-6.
- [13] Deng F, Li X, Lv X, et al. Low-Temperature Processing All-Inorganic Carbon-Based Perovskite Solar Cells up to 11.78% Efficiency via Alkali Hydroxides Interfacial Engineering [J]. *ACS Applied Energy Materials*, 2019, 3(1): 401-10.
- [14] Guo Y, Zhao F, Tao J, et al. Efficient and Hole-Transporting-Layer-Free CsPbI<sub>2</sub> Br Planar Heterojunction Perovskite Solar Cells through Rubidium Passivation [J]. *ChemSusChem*, 2019, 12(5): 983-9.
- [15] Gong S, Li H, Chen Z, et al. CsPbI<sub>2</sub>Br Perovskite Solar Cells Based on Carbon Black-Containing Counter Electrodes [J]. *ACS Applied Materials & Interfaces*, 2020, 12(31): 34882-9.
- [16] Guo Z, Zhao S, Liu A, et al. Niobium Incorporation into CsPbI<sub>2</sub>Br for Stable and Efficient All-Inorganic Perovskite Solar Cells [J]. *ACS Appl Mater Interfaces*, 2019, 11(22): 19994-20003.
- [17] Liu C, Wu M, Wu Y, et al. Efficient all-inorganic CsPbI<sub>2</sub>Br perovskite solar cell with carbon electrode by revealing crystallization kinetics and improving crystal quality [J]. *Journal of Power Sources*, 2020, 447: 227389.
- [18] Meng X, Wang Z, Qian W, et al. Excess Cesium Iodide Induces Spinodal Decomposition of CsPbI<sub>2</sub>Br Perovskite Films [J]. *The journal of physical chemistry letters*, 2019, 10(2): 194-9.
- [19] Ye Z, Zhou J, Hou J, et al. Low Temperature-Processed Stable and Efficient Carbon-Based CsPbI<sub>2</sub>Br Planar Perovskite Solar Cells by In Situ Passivating Grain Boundary and Trap Density [J]. *Solar RRL*, 2019, 3(8): 1900109.
- [20] Zhang X, Zhou Y, Li Y, et al. Efficient and carbon-based hole transport layer-free CsPbI<sub>2</sub>Br planar perovskite solar cells using PMMA modification [J]. *Journal of Materials Chemistry C*, 2019, 7(13): 3852-61.
- [21] Zhou Y, Zhang X, Lu X, et al. Promoting the Hole Extraction with Co<sub>3</sub>O<sub>4</sub> Nanomaterials for Efficient Carbon-Based CsPbI<sub>2</sub>Br Perovskite Solar Cells [J]. *Solar RRL*, 2019, 3(4): 1800315.
- [22] Zhu W, Chai W, Chen D, et al. High-Efficiency (>14%) and Air-Stable Carbon-Based, All-Inorganic CsPbI<sub>2</sub>Br Perovskite Solar Cells through a Top-Seeded Growth Strategy [J]. *ACS Energy Letters*, 2021: 1500-10.
- [23] Dong C, Han X, Li W, et al. Anti-solvent assisted multi-step deposition for efficient and stable carbon-based CsPbI<sub>2</sub>Br all-inorganic perovskite solar cell [J]. *Nano Energy*, 2019, 59: 553-9.
- [24] Guo Z, Teo S, Xu Z, et al. Achievable high Voc of carbon based all-inorganic CsPbI<sub>2</sub>Br perovskite solar cells through interface engineering [J]. *Journal of Materials Chemistry A*, 2019, 7(3): 1227-32.
- [25] Liang J, Liu Z, Qiu L, et al. Enhancing Optical, Electronic, Crystalline, and Morphological Properties of Cesium Lead Halide by Mn Substitution for High-Stability All-Inorganic Perovskite Solar Cells with Carbon Electrodes [J]. *Advanced Energy Materials*, 2018, 8(20).
- [26] Liang J, Zhao P, Wang C, et al. CsPb<sub>0.9</sub>Sn<sub>0.1</sub>I<sub>2</sub>Br<sub>2</sub> Based All-Inorganic Perovskite Solar Cells with Exceptional Efficiency and Stability [J]. *J Am Chem Soc*, 2017, 139(40): 14009-12.
- [27] Tan X, Liu X, Liu Z, et al. Enhancing the optical, morphological and electronic properties of the solution-processed CsPbI<sub>2</sub>Br films by Li doping for efficient carbon-based perovskite solar cells [J]. *Applied Surface Science*, 2020, 499.
- [28] Wang C, Zhang J, Jiang L, et al. All-inorganic, hole-transporting-layer-free, carbon-based CsPbI<sub>2</sub>Br planar solar cells with ZnO as electron-transporting materials [J]. *Journal of Alloys and Compounds*, 2020, 817.

- [29] Zhu W, Zhang Q, Chen D, et al. Intermolecular Exchange Boosts Efficiency of Air-Stable, Carbon-Based All-Inorganic Planar CsPbIBr<sub>2</sub> Perovskite Solar Cells to Over 9% [J]. *Advanced Energy Materials*, 2018, 8(30).
- [30] Zhu W, Zhang Q, Zhang C, et al. Aged Precursor Solution toward Low-Temperature Fabrication of Efficient Carbon-Based All-Inorganic Planar CsPbIBr<sub>2</sub> Perovskite Solar Cells [J]. *ACS Applied Energy Materials*, 2018, 1(9): 4991-7.
- [31] Zhu W, Zhang Z, Chai W, et al. Benign Pinholes in CsPbIBr<sub>2</sub> Absorber Film Enable Efficient Carbon-Based, All-Inorganic Perovskite Solar Cells [J]. *ACS Applied Energy Materials*, 2019, 2(7): 5254-62.
- [32] Chang X, Li W, Zhu L, et al. Carbon-Based CsPbBr<sub>3</sub> Perovskite Solar Cells: All-Ambient Processes and High Thermal Stability [J]. *ACS Appl Mater Interfaces*, 2016, 8(49): 33649-55.
- [33] Teng P, Han X, Li J, et al. Elegant Face-Down Liquid-Space-Restricted Deposition of CsPbBr<sub>3</sub> Films for Efficient Carbon-Based All-Inorganic Planar Perovskite Solar Cells [J]. *ACS Appl Mater Interfaces*, 2018, 10(11): 9541-6.
- [34] Liu J, Zhu L, Xiang S, et al. Growing high-quality CsPbBr<sub>3</sub> by using porous CsPb<sub>2</sub>Br<sub>5</sub> as an intermediate: a promising light absorber in carbon-based perovskite solar cells [J]. *Sustainable Energy & Fuels*, 2019, 3(1): 184-94.
- [35] Du J, Duan J, Yang X, et al. p-Type Charge Transfer Doping of Graphene Oxide with (NiCo)<sub>1-y</sub>FeyO<sub>x</sub> for Air-Stable, All-Inorganic CsPbIBr<sub>2</sub> Perovskite Solar Cells [J]. *Angewandte Chemie International Edition*, 2021, n/a(n/a).
- [36] Liang J, Wang C, Wang Y, et al. All-Inorganic Perovskite Solar Cells [J]. *J Am Chem Soc*, 2016, 138(49): 15829-32.
- [37] Cao X, Zhang G, Jiang L, et al. Water, a Green Solvent for Fabrication of High-Quality CsPbBr<sub>3</sub> Films for Efficient Solar Cells [J]. *ACS Appl Mater Interfaces*, 2020, 12(5): 5925-31.
- [38] Wang G, Dong W, Gurung A, et al. Improving photovoltaic performance of carbon-based CsPbBr<sub>3</sub> perovskite solar cells by interfacial engineering using P3HT interlayer [J]. *Journal of Power Sources*, 2019, 432: 48-54.
- [39] Liu X, Liu Z, Tan X, et al. Novel antisolvent-washing strategy for highly efficient carbon-based planar CsPbBr<sub>3</sub> perovskite solar cells [J]. *Journal of Power Sources*, 2019, 439.
- [40] Liu X, Tan X, Liu Z, et al. Boosting the efficiency of carbon-based planar CsPbBr<sub>3</sub> perovskite solar cells by a modified multistep spin-coating technique and interface engineering [J]. *Nano Energy*, 2019, 56: 184-95.
- [41] Tang M, He B, Dou D, et al. Toward efficient and air-stable carbon-based all-inorganic perovskite solar cells through substituting CsPbBr<sub>3</sub> films with transition metal ions [J]. *Chemical Engineering Journal*, 2019, 375.
- [42] Liu Y, He B, Duan J, et al. Poly(3-hexylthiophene)/zinc phthalocyanine composites for advanced interface engineering of 10.03%-efficiency CsPbBr<sub>3</sub> perovskite solar cells [J]. *Journal of Materials Chemistry A*, 2019, 7(20): 12635-44.
- [43] Zhao Y, Duan J, Yuan H, et al. Using SnO<sub>2</sub> QDs and CsMBr<sub>3</sub>(M = Sn, Bi, Cu) QDs as Charge-Transporting Materials for 10.6%-Efficiency All-Inorganic CsPbBr<sub>3</sub> Perovskite Solar Cells with an Ultrahigh Open-Circuit Voltage of 1.610 V [J]. *Solar RRL*, 2019, 3(3).
- [44] Duan J, Zhao Y, Yang X, et al. Lanthanide Ions Doped CsPbBr<sub>3</sub> Halides for HTM-Free 10.14%-Efficiency Inorganic Perovskite Solar Cell with an Ultrahigh Open-Circuit Voltage of 1.594 V [J]. *Advanced Energy Materials*, 2018, 8(31).
- [45] Zhao Y, Duan J, Wang Y, et al. Precise stress control of inorganic perovskite films for carbon-based solar cells with an ultrahigh voltage of 1.622 V [J]. *Nano Energy*, 2020, 67.
- [46] Duan J, Zhao Y, Wang Y, et al. Hole-Boosted Cu(Cr,M)O<sub>2</sub> Nanocrystals for All-Inorganic CsPbBr<sub>3</sub> Perovskite Solar Cells [J]. *Angew Chem Int Ed Engl*, 2019, 58(45): 16147-51.
- [47] Duan J, Wang Y, Yang X, et al. Alkyl-Chain-Regulated Charge Transfer in Fluorescent Inorganic CsPbBr<sub>3</sub> Perovskite Solar Cells [J]. *Angew Chem Int Ed Engl*, 2020.
- [48] Liao G, Zhao Y, Duan J, et al. Enhanced charge extraction with all-carbon electrodes for inorganic CsPbBr<sub>3</sub> perovskite solar cells [J]. *Dalton Trans*, 2018, 47(43): 15283-7.
- [49] Wu Y, Wang Y, Duan J, et al. Cluster effect of additives in precursors for inorganic perovskites solar cells [J]. *Electrochimica Acta*, 2020, 331.
- [50] Zhao Y, Liu T, Ren F, et al. Organic hole-transporting materials for 9.32%-efficiency and stable CsPbBr<sub>3</sub> perovskite solar cells [J]. *Materials Chemistry Frontiers*, 2018, 2(12): 2239-44.
- [51] Duan J, Zhao Y, He B, et al. High-purity inorganic perovskite films for solar cells with 9.72% efficiency [J]. *Angewandte chemie international edition*, 2018, 57(14): 3787-91.
- [52] Zhao B, Jin S-F, Huang S, et al. Thermodynamically Stable Orthorhombic  $\gamma$ -CsPbI<sub>3</sub> Thin Films for High-Performance Photovoltaics [J]. *Journal of the American Chemical Society*, 2018, 140(37): 11716-25.